

Analysis and Experiment of Equilateral Triangular Uniaxial-Anisotropic Dielectric Resonator Antennas

*Original*

Analysis and Experiment of Equilateral Triangular Uniaxial-Anisotropic Dielectric Resonator Antennas / Fakhte, S.; Aryanian, I.; Matekovits, L.. - In: IEEE ACCESS. - ISSN 2169-3536. - ELETTRONICO. - 6:1(2018), pp. 63071-63079. [10.1109/ACCESS.2018.2877121]

*Availability:*

This version is available at: 11583/2717451 since: 2018-11-16T14:31:59Z

*Publisher:*

Institute of Electrical and Electronics Engineers Inc.

*Published*

DOI:10.1109/ACCESS.2018.2877121

*Terms of use:*

This article is made available under terms and conditions as specified in the corresponding bibliographic description in the repository

*Publisher copyright*

(Article begins on next page)

Received September 22, 2018, accepted October 9, 2018, date of publication October 23, 2018, date of current version November 14, 2018.

Digital Object Identifier 10.1109/ACCESS.2018.2877121

# Analysis and Experiment of Equilateral Triangular Uniaxial-Anisotropic Dielectric Resonator Antennas

SAEED FAKHTE<sup>1,2</sup>, IMAN ARYANIAN<sup>1</sup>,  
AND LADISLAV MATEKOVITS<sup>2,3</sup>, (Senior Member, IEEE)

<sup>1</sup>Iran Telecommunication Research Center, Tehran 14155-3961, Iran

<sup>2</sup>Department of Electronics and Telecommunications, Politecnico di Torino, 10129 Torino, Italy

<sup>3</sup>School of Engineering, Macquarie University, Sydney, NSW 2109, Australia

Corresponding author: Saeed Fakhte (s.fakhte@itrc.ac.ir)

This work was supported by the Iran Telecommunication Research Center (ITRC), Tehran, Iran.

**ABSTRACT** The design procedure of a uniaxial anisotropic equilateral triangular dielectric resonator antenna (ETDRA) is presented for the first time. The uniaxial material is realized by a periodic stack of sheets of two dissimilar materials with different dielectric constants. It is proven that the increase of the boresight gain and impedance bandwidth of the ETDRA is possible by using the uniaxial material for the antenna prism. The gain improvement is due to the increase in the sidewall radiations and the bandwidth enhancement is owing to the lowering of the effective permittivity of the structure. The fabricated anisotropic ETDRA offers an impedance bandwidth of 27.7% between 3.025 and 4 GHz with a measured gain above 8 dB. The simulation results agree well with the experimental ones.

**INDEX TERMS** Gain, fundamental mode, impedance bandwidth, equilateral triangular dielectric resonator antenna (ETDRA).

## I. INTRODUCTION

Over the last few decades, the dielectric resonator antenna (DRA) has been drawing enormous attention to prompt significant progress in microwave and millimeter wave antenna technologies. The dielectric resonator antennas have offered several advantages such as high efficiency, light weight, compact size, low cost and shape versatility [1]–[3]. These days, DRAs become a feasible alternative to conventional low-gain elements such as microstrip patches, dipoles and monopoles [4]. Triangular DRA has the advantage over the rectangular and circular ones of having smallest size when the DRAs have the same dielectric constant, height and operating frequency [5]–[8].

Modern communications set the bandwidth requirement high and the DRA technology, even if of wideband by nature, needs to keep up with it. Some efforts have been devoted to developing wideband triangular DRAs [9], [10]. In [9], two different modes of the ETDRA have been combined to give a wideband design. In [10], a new feeding mechanism based on a conducting conformal strip has been adopted to fulfill the requested impedance match bandwidth.

DRAs operating in their lowest order modes all radiate like short magnetic or electric dipoles. Mounting them on a

moderate to large ground plane results in the generation of the radiation patterns with the maximum directivity of about 5dB [2]. There are some published works on the triangular dielectric resonator antennas (TDRAs) with enhanced gain [9], [11]. In [9], by exciting the higher order mode of the TDRA, a gain increase of up to 7.5 dB has been achieved. Also, in [11], the increased gain has been obtained by arraying the TDRAs.

However, a limited number of papers on wideband and enhanced gain ETDRA has been reported so far. Therefore, there is still much room for development in this field.

Theoretical and experimental investigations have been reported on rectangular [12]–[14], and cylindrical [15] shaped anisotropic DRAs; however, at the best of the authors' knowledge, the anisotropic triangular DRA has not yet been explored. It has been reported that, by using the uniaxial anisotropic material, with the tensor ratio of  $\epsilon_z/\epsilon_x$  smaller than one, inside the rectangular DRA [13] and cylindrical DRA [15], the intensity of the radiated fields from their sidewalls compared to those of their top wall will be augmented which in turn enhances their boresight gain. The aforementioned uniaxial anisotropic material is realized by a periodic stack of multiple layers of two dissimilar dielectric

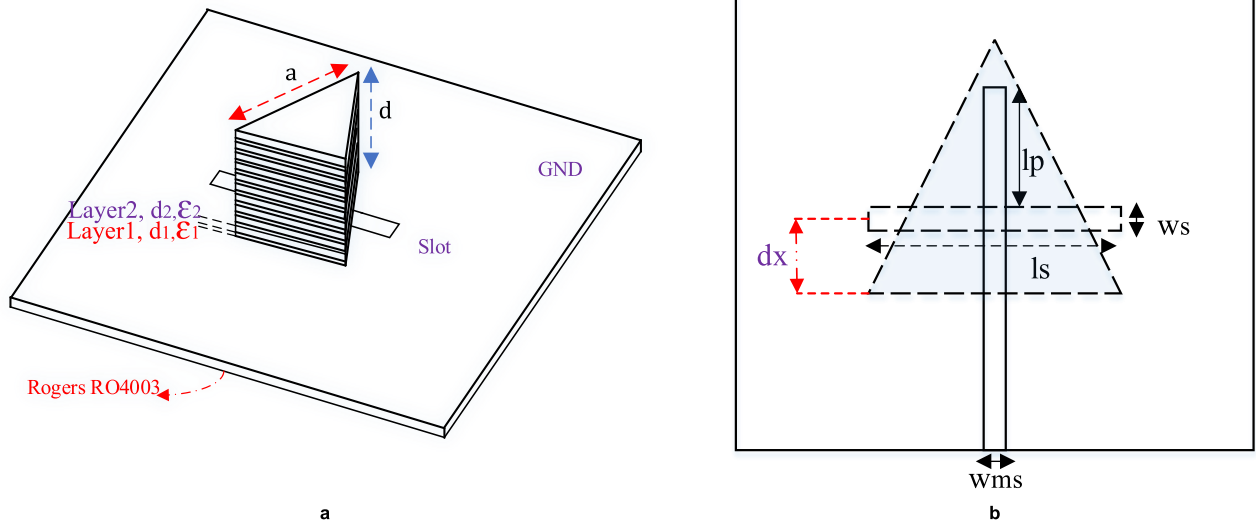


FIGURE 1. The configuration of the proposed equilateral triangular uniaxial-anisotropic DRA, (a) 3D view, (b) Bottom view.

sheets with different dielectric constants [16], [17]. Note that, to achieve the low tensor ratio of  $\epsilon_z/\epsilon_x$ , the low permittivity layers should be sandwiched between the high permittivity ones, which lowers the effective permittivity of the antenna (built with the only high permittivity material) and enhances its impedance bandwidth.

In this paper, for the first time, a uniaxial anisotropic equilateral triangular DRA is investigated both theoretically and experimentally. Using the theoretical model described in [8] for the isotropic ETDRA, the electric and magnetic fields inside the anisotropic ETDRA are derived. Then, the design formula of the  $TM_{101}^z$  mode of the uniaxial anisotropic ETDRA is obtained by using perfect magnetic wall assumption. It is concluded that, by decreasing the ratio of  $\epsilon_z/\epsilon_x$ , one can increase the boresight gain of the antenna. Also, it results in a noticeable enhancement in the impedance bandwidth results. To explain the reason behind the high gain nature of the anisotropic ETDRA, the far-field electric component of the radiation patterns of the different walls of the anisotropic ETDRA are analytically calculated. The proposed antenna is fabricated and measured. The measured and simulated results show an increase in the boresight gain and impedance bandwidth of the antenna. The simulations agree well with the measurements.

Note that, the smaller size of the anisotropic ETDRA compared to the rectangular [13] and cylindrical [15] anisotropic DRA is an advantage for the anisotropic ETDRA, as it was already mentioned for the isotropic ones [5]–[8].

This paper is organized as follows: in Section II the antenna configuration is described and the method for realizing the anisotropic ETDRA is explained in more detail. Also, the mechanism of gain improvement of the anisotropic ETDRA is discussed. In Section III, the measured results of the fabricated prototype are discussed. Finally, Section IV is devoted to the conclusion of this work.

## II. ANTENNA CONFIGURATION

Figure 1 shows the proposed DRA configuration, where a multilayer ETDRA resides on a  $90\text{mm} \times 90\text{mm}$  ground plane on a RO4003 substrate of thickness  $0.508\text{ mm}$  and permittivity  $3.38$  and excited by a slot aperture of length  $l_s$  and width  $w_s$ . A  $50\ \Omega$  microstrip line ( $w_{ms} = 1.15\text{ mm}$ ) is used to feed the DRA through the aperture. The microstrip line is extended over the aperture by a length  $l_p$ . The antenna is a periodic stack of ten layers of Rogers RT5870 ( $\epsilon_{r1} = 2.33, \tan\delta_1 = 0.0012, d_1 = 0.787\text{ mm}$ ) and ten layers of Rogers RT6010 ( $\epsilon_{r2} = 10.2, \tan\delta_2 = 0.0023, d_2 = 1.27\text{ mm}$ ). With reference to Fig. 1, the layers are parallel to the XY plane, and periodic along the z axis. When the thickness of the layers is small compared to the wavelength, the stacked structure behaves as a homogeneous anisotropic material with the following equivalent diagonal permittivity tensor [16]–[17].

$$\epsilon_x = \epsilon_y = \frac{\epsilon_1\epsilon_2(d_1 + d_2)}{\epsilon_1d_1 + \epsilon_2d_2} \quad \epsilon_z = \frac{\epsilon_1d_2 + \epsilon_2d_1}{d_1 + d_2}$$

$$\epsilon_r = \begin{pmatrix} 7.19 & 0 & 0 \\ 0 & 7.19 & 0 \\ 0 & 0 & 4.45 \end{pmatrix} \quad (1)$$

Using the method reported in [8], the electric and magnetic field components of the  $TM_{101}^z$  mode inside the anisotropic ETDRA are obtained as follows

$$E_x = E_{z0} \frac{\epsilon_z}{\epsilon_x} \frac{2Ak_z}{\chi^2} \sin(A(x + R)) \cos(By) \cos(k_z(d - z)) \quad (2)$$

$$E_y = E_{z0} \frac{\epsilon_z}{\epsilon_x} \frac{2Bk_z}{\chi^2} [\cos(A(x + R)) \sin(By) + \sin(2By)] \cos(k_z(d - z)) \quad (3)$$

$$E_z = E_{z0} [2 \cos(A(x + R)) \cos(By) + \cos(2By)] \sin(k_z(d - z)) \quad (4)$$

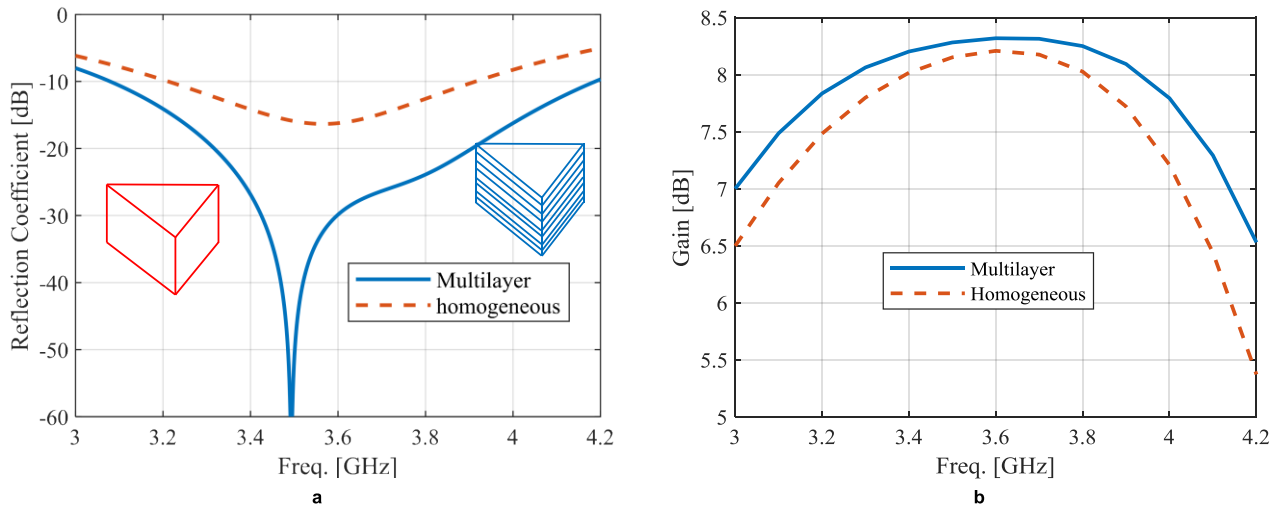


**FIGURE 2.** Comparison between the simulated results of the multilayer ETDR and its homogeneous anisotropic counterpart, (a) reflection coefficient, (b) gain.

$$H_x = -jE_{z0} \frac{2B\omega\epsilon_0\epsilon_z}{\chi^2} [\cos(A(x+R)) \sin(By) + \sin(2By)] \sin(k_z(d-z)) \quad (5)$$

$$H_y = jE_{z0} \frac{2A\omega\epsilon_0\epsilon_z}{\chi^2} \sin(A(x+R)) \cos(By) \sin(k_z(d-z)) \quad (6)$$

$$H_z = 0 \quad (7)$$

Where  $A = \frac{2\pi}{\sqrt{3}a}$ ,  $B = \frac{2\pi}{3a}$ ,  $\chi = \frac{4\pi}{3a}$ ,  $k_z = \frac{\pi}{2d}$ ,  $R = \frac{a}{\sqrt{3}}$ , and  $\omega = 2\pi f_r$ . Other parameters are as shown in Fig. 1. Note that all the walls of the ETDR are assumed to be perfect magnetic conductors (PMCs).

The following approximate design formula is used to obtain the primary design parameters, which are subsequently optimized using the simulation results,

$$f_r = \frac{c}{2\pi\sqrt{\epsilon_z}} \sqrt{\chi^2 + \frac{\epsilon_z}{\epsilon_x} k_z^2} \quad (8)$$

where  $c$  is the speed of light and the other parameters are defined above. Note that, since the permittivity tensor elements along the X and Y directions are equal, the resonant frequency depends only on  $\epsilon_z$  and  $\epsilon_x$ . This formula is derived from the dispersion equation, which is calculated by substituting Eqs. (2-7) into Maxwell equations. The accuracy of this formula can be further increased by using the effective dimensions of the ETDR operating at  $TM_{101}^z$  mode as reported in [8, eq. (23-24)], Note that, in these equations,  $\epsilon_r$  is replaced by  $\epsilon_r = (\epsilon_x + \epsilon_z)/2$ .

The optimized dimensions of the proposed antenna in terms of the optimum gain and impedance bandwidth are as follows:  $a = 38.4$ , mm,  $d = 20.57$ , mm,  $l_s = 42.1$  mm,  $l_p = 16.4$ , mm,  $w_s = 1.6$  mm. By substituting the value of these parameters in (8) the predicted resonant frequency for the  $TM_{101}^z$  mode is 3.7 GHz.

To confirm that the uniaxial anisotropic ETDR can be realized by the dielectric stacking method, the simulation

results of the multilayer ETDR and that of a homogeneous anisotropic ETDR with the dielectric constant tensor of (1) and the same dimensions as those of the multilayer one are compared. From simulations, it is apparent that the  $TM_{101}^z$  mode resonant frequency of the multilayer and homogeneous anisotropic ETDRs are 3.5 GHz and 3.55 GHz, respectively, which are very close to each other. Note that, in multilayer ETDR, the slot aperture is in contact with the first layer which is the dielectric layer with low permittivity (Rogers 5870,  $\epsilon_{r1} = 2.33$ ,  $d_1 = 0.787$  mm), unlike the homogeneous structure, in which the slot aperture is directly in contact with the anisotropic medium. So, one can expect that, even though both the homogeneous and multilayer anisotropic ETDRs should resonate at nearly the same frequency, their impedance matching level may be different, as shown in Fig. 2(a). Also, the inconsistency between the simulated gains of the multilayer and homogeneous structures can be ascribed to the first layer effect (Fig. 2(b)). So, to prove that the first layer is responsible for the aforementioned inconsistencies between the simulated results, the multilayer structure is modeled as the homogeneous anisotropic ETDR placed on the layer1, as depicted in the inset of Fig. 3(a). Observe in Figs. 3(a) and (b) that, now the simulated reflection coefficients and gains of the multilayer ETDR and its modified homogeneous anisotropic counterpart are very close to each other.

Note that, it appears in Fig. 3 that the antenna has 8.3 dB peak gain, which is relatively high for a dielectric resonator antenna operating at its fundamental radiating mode [2]. Thus, to explore the reason behind the high gain nature of this antenna, a theoretical study of the far-field radiation patterns is carried out. But before proceeding, for a fair comparison, an isotropic ETDR with the same aspect ratio as that of the anisotropic ETDR ( $\frac{d}{a} = 0.536$ ) and filled with the isotropic material (Rogers RT6010,  $\epsilon_{r2} = 10.2$ ,  $\tan\delta = 0.0023$ ) is designed. With reference to Fig. 1, the optimized dimen-

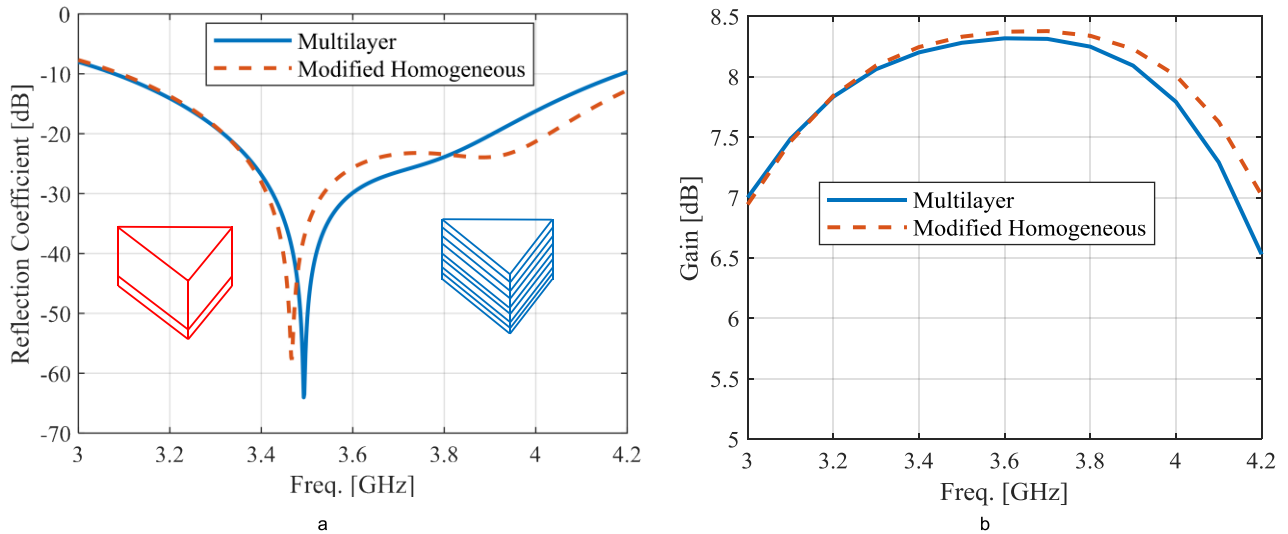


FIGURE 3. Comparison between the simulated results of the multilayer ETDR and its modified homogeneous anisotropic counterpart, (a) reflection coefficient, (b) gain.

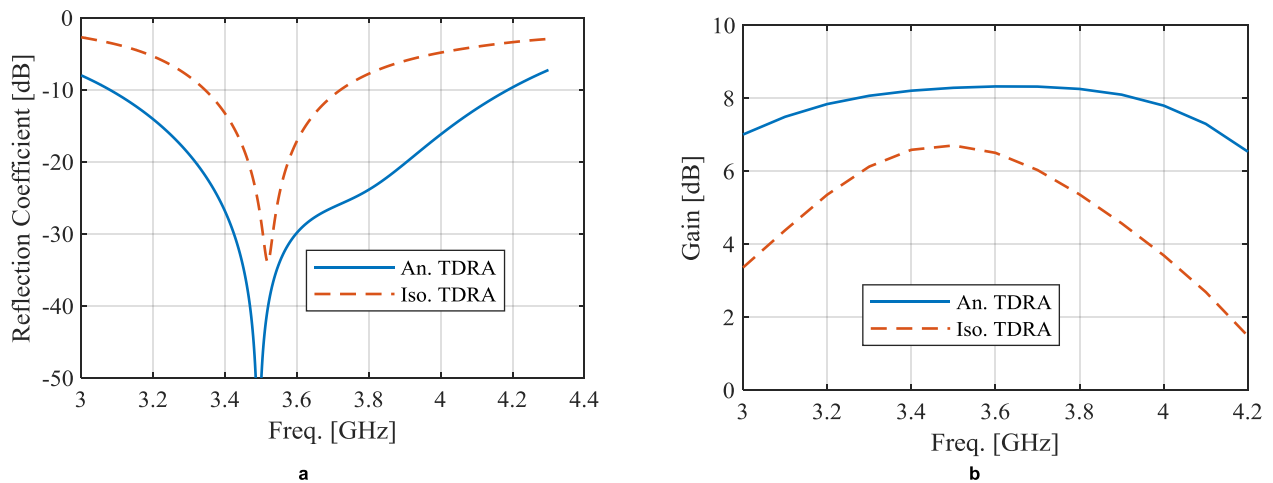


FIGURE 4. simulated results of the isotropic and anisotropic ETDRAs, (a) reflection coefficient, (b) gain.

sions of the isotropic ETDR and its feeding network are as follows:  $a = 30$ , mm,  $d = 16.07$ , mm,  $l_s = 42.1$ , mm,  $l_p = 11$ , mm,  $w_s = 1.6$  mm. Figure 4 shows the comparison between the simulated results (reflection coefficient and gain) of these two samples. As expected, the results show that the anisotropic ETDR has a wider impedance bandwidth and higher gain compared to the isotropic one. The bandwidth enhancement of the anisotropic ETDR is owing to the reduction in the overall permittivity of the antenna. Also, the enhanced gain of the anisotropic ETDR is because of the increase in the sidewall-to-top wall radiation ratio of the antenna compared to the isotropic sample.

Figure 5 shows the simulated electric field distributions of the isotropic and anisotropic ETDRAs at 3.5 GHz, where both the antennas resonate. It is evident from this figure that the sidewall-to-top wall radiation of the anisotropic ETDR

is greater than that of the isotropic one. This fact can also be confirmed by comparing the  $E_z$  component in Eq. (4), to the  $E_x$  and  $E_y$  components in Eqs. (2-3). It is apparent that by employing the uniaxial material with  $\epsilon_z$ -to- $\epsilon_x$  ratio smaller than one (here,  $\epsilon_z/\epsilon_x = 0.62$ ) inside the ETDR prism, the magnitude of the electric field in the  $z$ -direction is increased compared to those of the  $x$ - and  $y$ -directions. Similar to the previous works for the rectangular and cylindrical anisotropic DRAs [13], [15], it can be theoretically proved that this is the reason behind the gain improvement of the anisotropic ETDR. The relationship between the boresight gain and the side-to-top wall radiation of the ETDR can be obtained via the following theoretical investigation.

For the theoretical study of the anisotropic ETDR, an infinite size perfect electric conductor is assumed as the ground plane of the antenna, and then, by using the image

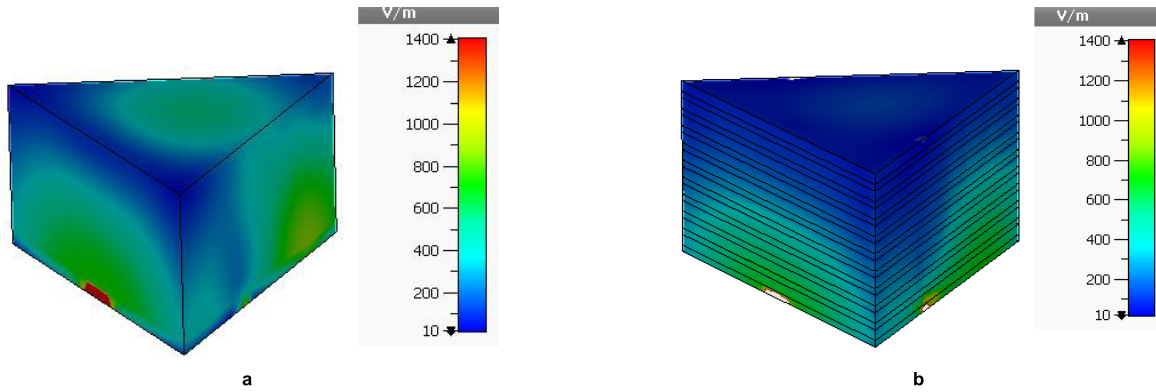


FIGURE 5. The electric field distributions at 3.5 GHz obtained by CST MW studio, (a) Isotropic ETDR, (b) Anisotropic ETDR.

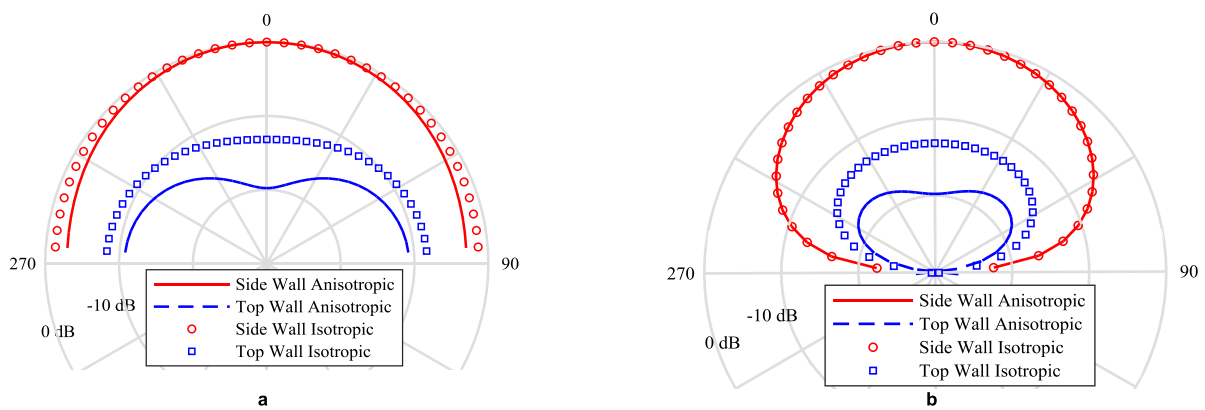


FIGURE 6. Theoretical radiation patterns originated from the walls of the iso- and anisotropic ETDRs at 3.5 GHz, (a) XZ plane, (b) YZ plane.

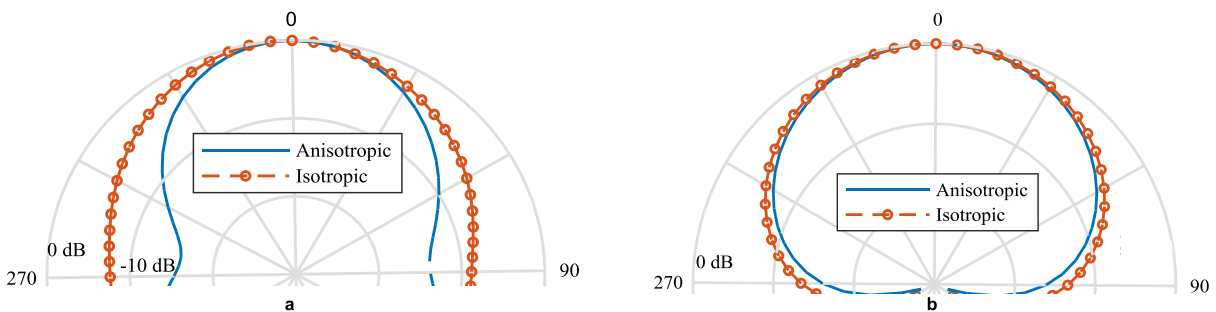


FIGURE 7. Radiation patterns of the isotropic and anisotropic ETDRs at 3.5 GHz obtained using CST Microwave Studio, (a) XZ (E-) plane, (b) YZ (H-) plane.

theorem, its far-field patterns are determined. Based on the surface equivalent theory (Huygens's Principle) [18], to calculate the far-field radiation patterns of the antenna, the ETDR can be modeled as the equivalent magnetic surface currents,  $M_s = \vec{E} \times \hat{n}$ , where  $\hat{n}$  is a unit normal pointing outward from the dielectric. Then, the far-field radiated electric fields can be calculated as follows [18]:

$$E_\theta \propto (L_\varphi^s + L_\varphi^{tb}) \quad (9)$$

$$E_\varphi \propto (L_\theta^s + L_\theta^{tb}) \quad (10)$$

where

$$L_\varphi^{s.tb} = -F_x^{s.tb} \sin(\varphi) + F_y^{s.tb} \cos(\varphi) \quad (11)$$

$$L_\theta^{s.tb} = F_x^{s.tb} \cos(\theta) \cos(\varphi) + F_y^{s.tb} \cos(\theta) \sin(\varphi) - F_z^{s.tb} \sin(\theta) \quad (12)$$

The superscripts  $s$  and  $tb$  represent the vector potentials originated by the sidewalls and top-bottom walls of the ETDR, respectively. The expressions of the scalar functions  $F$  above,

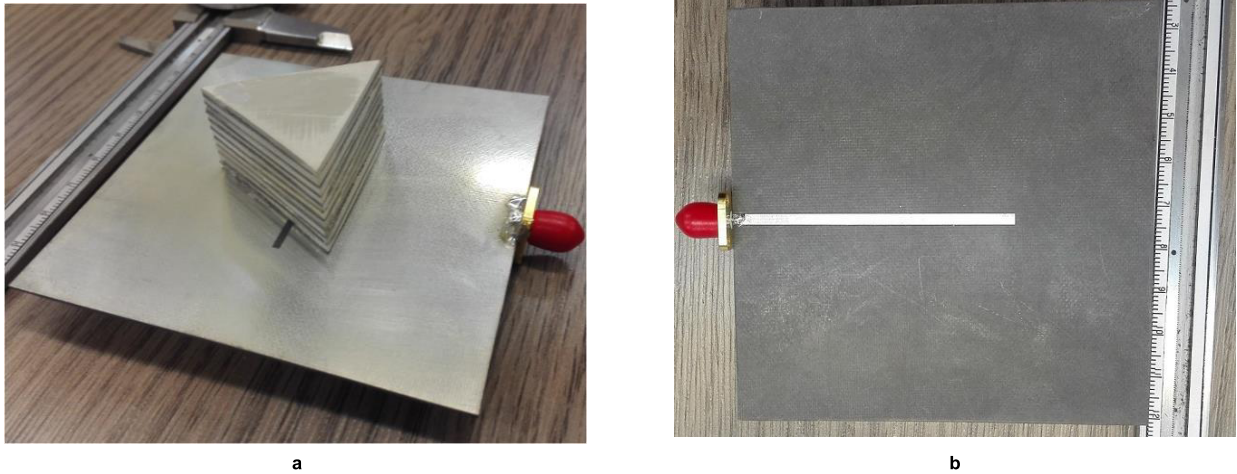


FIGURE 8. Photograph of the fabricated prototype of the proposed antenna, (a) 3D view, (b) the bottom view.

are as follows:

$$F_x^s = 4\pi dE_{z0} (I_{AB}^x - I_{AC}^x) \frac{\cos(dk_0 \cos(\theta))}{\pi^2 - 4d^2 k_0^2 \cos^2(\theta)} \quad (13)$$

$$F_x^{tb} = -2k_z \frac{E_{z0}}{\chi^2} \frac{\varepsilon_z}{\varepsilon_x} I_{cs} \cos(dk_0 \cos(\theta)) \quad (14)$$

$$F_y^s = -4\pi dE_{z0} \frac{\cos(dk_0 \cos(\theta))}{\pi^2 - 4d^2 k_0^2 \cos^2(\theta)} \times \left\{ \frac{I_{AC}^x + I_{AB}^x}{\sqrt{3}} - e^{j\frac{\sqrt{3}}{2} a k_0 \sin(\theta) \cos(\varphi)} I_{BC}^y \right\} \quad (15)$$

$$F_y^{tb} = 2k_z \frac{E_{z0}}{\chi^2} \frac{\varepsilon_z}{\varepsilon_x} I_{sc} \cos(dk_0 \cos(\theta)) \quad (16)$$

$$F_z^s = -4\pi d j \frac{1}{\chi^2} \frac{\varepsilon_z}{\varepsilon_x} E_{z0} \times \left[ \left( \frac{4}{3} \right) (I_{AC}^{zx} - I_{AB}^{zx}) - e^{j\frac{\sqrt{3}}{2} a k_0 \sin(\theta) \cos(\varphi)} I_{BC}^z \right] \cdot \frac{k_0 \cos(\theta) \cos(dk_0 \cos(\theta))}{\pi^2 - 4d^2 k_0^2 \cos^2(\theta)} \quad (17)$$

$$F_z^{tb} = 0 \quad (18)$$

where  $I_{AB}^x, I_{AC}^x, I_{cs}, I_{sc}, I_{BC}^y$ , and  $I_{BC}^z$  are defined in [8] and are omitted here for brevity.

The theoretical radiation patterns originated from the walls of the iso- and aniso-tropic ETDRAs in the XZ and YZ planes are drawn in Fig. 6. Note that, the  $E_\theta$  and  $E_\varphi$  are the dominant components of the electric field in the XZ- and YZ- planes, respectively, which can also be deduced from Eqs. (9-17). Observe in Fig. 6(a) that the far-field  $E_\theta$  patterns arising from the side walls of both the iso- and aniso-tropic ETDRAs,  $E_\theta \propto L_\varphi^s$ , have their maximum values in the  $\theta = 0^\circ$  direction, but those of the top and bottom walls,  $E_\theta \propto L_\varphi^{tb}$ , are not directive in this direction. This behavior is due to the field distribution of the  $TM_{101}^z$  mode in the anisotropic ETDRAs and is resulted from eqs. (11-17). Therefore, to achieve a highly directive radiation pattern,  $E_\theta \propto (L_\varphi^s + L_\varphi^{tb})$ , the radiation

intensity due to the sidewalls (directive one),  $L_\varphi^s$ , compared to that of the top-bottom walls,  $L_\varphi^{tb}$ , should be increased.

To attain this goal, the uniaxial material is used inside the ETDRAs prism. Then, from Eqs. (13) and (14) one can see that decreasing the  $\varepsilon_z/\varepsilon_x$  ratio leads to an increase in the magnitude of the  $F_x^s$  compared to that of the  $F_x^{tb}$  and the magnitude of the  $F_y^s$  compared to the  $F_y^{tb}$ . So, observe in Fig. 6(a) that by lowering the  $\varepsilon_z/\varepsilon_x$  ratio from 1 for the isotropic ETDRAs to 0.62 for the anisotropic ETDRAs the radiation pattern due to the sidewalls of the antenna becomes narrower and the difference between the levels of the radiation patterns due to the side walls (directive one) and top-bottom walls is increased.

Also, the theoretical results of the YZ radiation patterns are drawn in Fig. 6(b). Note that, the radiation pattern originated from the top-bottom walls of the isotropic ETDRAs is already directive and decreasing its level compared to that of the sidewalls does not change the total pattern considerably.

To further verify that the narrowing of the XZ (E-) plane radiation beam is the reason of the gain enhancement of the anisotropic antenna. The simulated XZ and YZ radiation patterns of the isotropic and anisotropic ETDRAs are plotted in Fig. 7. As discussed above in the theoretical study, one can see in Fig. 7 that by using anisotropic uniaxial material ( $\varepsilon_x = 7.19, \varepsilon_z = 4.45$ ) inside the ETDRAs, the beamwidth in XZ plane becomes narrower and that of the YZ plane does not change considerably. As mentioned before, this happens because of the special field distribution of the  $TM_{101}^z$  mode in the ETDRAs.

### III. MEASURED RESULTS

The fabricated structure for the antenna in Fig. 1 appears in Fig. 8 with the optimal design parameters. The measured and simulated reflection coefficients are drawn in Fig. 9(a). The measured result shows a wide impedance bandwidth of 27.7% (3.025-4 GHz), covering the WIMAX band (3.4-3.7 GHz). Since the existence of the air gap between

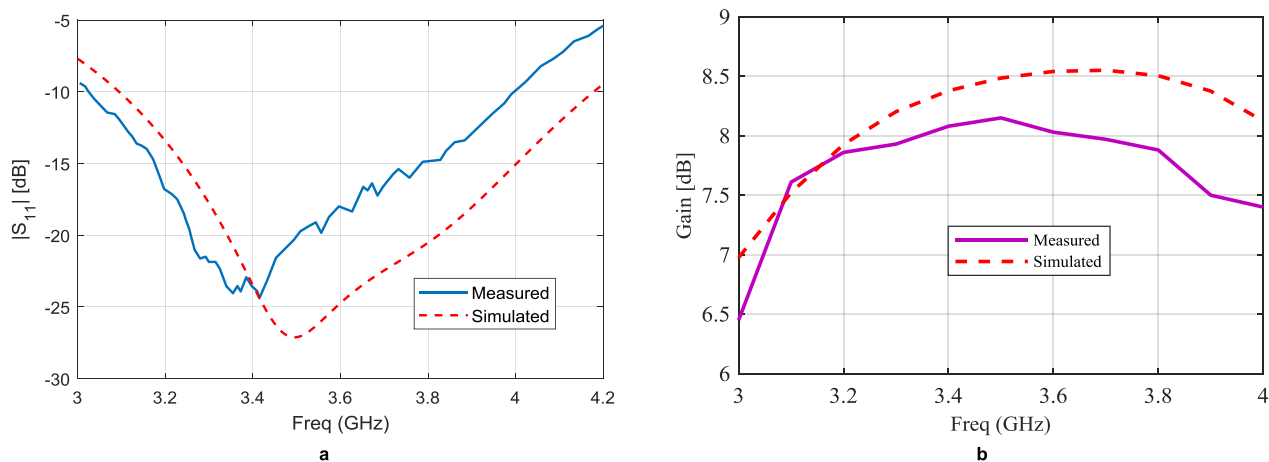


FIGURE 9. The measured and simulated results of the fabricated antenna, (a) Reflection coefficient, (b) Gain.

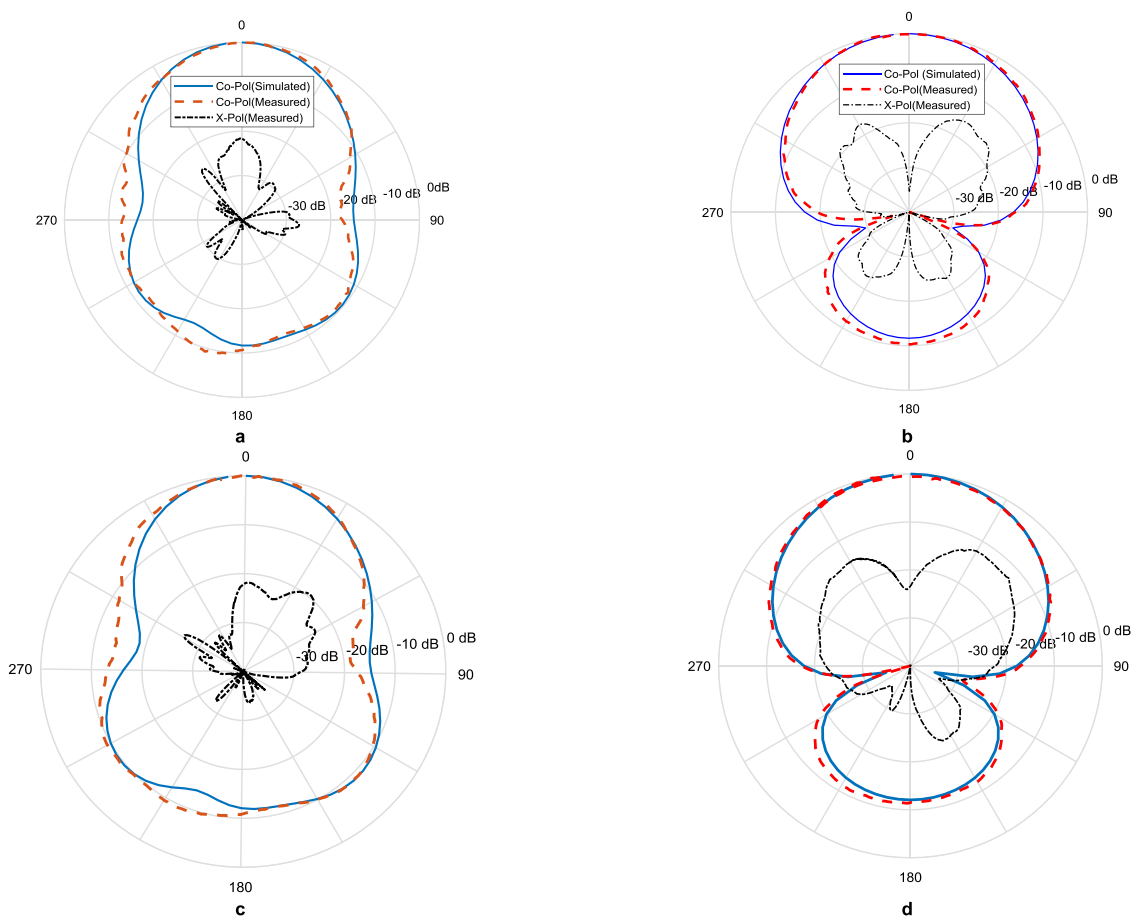


FIGURE 10. The measured and simulated radiation patterns of the proposed antenna, (a) XZ plane at 3.5 GHz, (b) YZ plane at 3.5 GHz, (c) XZ plane at 3.7 GHz, (d) YZ plane at 3.7 GHz.

the layers of the antenna is unavoidable, its effect on the reflection coefficient should be studied [19]–[21]. It is found that by considering the value of 0.02 mm for the air gap thickness, the simulation results show good agreement with the measured data. The curves are not included for brevity. However, still, an inconsistency between the measured and

simulation results is observed which is due to the fabrication errors. Moreover, there is another minimum in the reflection coefficient curve at 3.7 GHz. By changing the slot length, it can be verified that this is due to the slot resonance. The parametric study on the slot length is not included here for the sake of brevity.

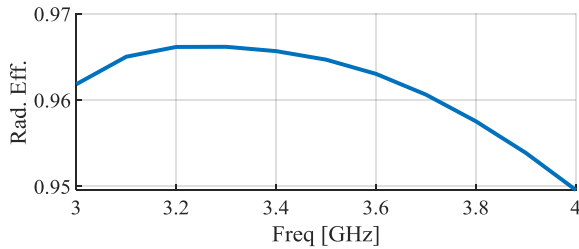


FIGURE 11. The radiation efficiency of the proposed antenna.

Also, the measured and simulated gains are plotted in Fig. 9(b). It shows that the proposed antenna has a maximum measured gain of 8.1 dB. This is about 2 dB higher than that of the isotropic ETDRA, as it can be seen in Fig. 4(b). This proves the predictions of the theory and simulation.

In [5], the maximum measured gain of the isotropic ETDRA is 5.2 dB which is about 2.9 dB lower than that of the anisotropic ETDRA presented in this work. In [9], the measured peak gain of the isotropic triangular DRA operating at its fundamental radiating mode is about 5 dB. But the peak measured gain of the anisotropic triangular DRA is 8.1 dB. So, a gain improvement of 3.1 dB is achieved.

The radiation patterns of the fabricated antenna are measured in an anechoic chamber. The measured and simulated radiation patterns in the XZ-plane (E-plane) and the YZ-plane (H-plane) at 3.5 and 3.7 GHz are drawn in Fig. 10. It can be noticed that the  $TM_{101}^z$  mode of the anisotropic ETDRA has a broadside radiation (Fig. 10(a) and (b)). As shown in Fig. 10(c) and (d), the radiation patterns at 3.7 GHz, where the slot resonates, are also broadside. (Observe that the maximums of the radiation patterns are in the  $\theta = 0^\circ$  direction.) Symmetrical radiation patterns with low cross-polarization levels (lower than  $-20$  dB in the boresight direction  $\theta = 0^\circ$ ) are observed in the measurements and simulations. Finally, observe in Fig. 11 that the simulated result of the radiation efficiency is higher than 95% over the whole bandwidth.

#### IV. CONCLUSION

The use of the uniaxial anisotropic material with the  $\epsilon_z/\epsilon_x$  ratio smaller than unity inside the triangular DRA prism improves the performance of the antenna. This idea is studied theoretically and verified experimentally in this work. It is shown that about 2 dB gain enhancement can be achieved using this technique. Also, a wideband antenna is obtained thanks to the reduction in the overall permittivity of the antenna. At the authors' best knowledge, this is the first anisotropic triangular DRA that has been studied until now.

#### ACKNOWLEDGMENT

This work has been partially supported by the project "Advanced Nonradiating Architectures Scattering Tenuously

and Sustaining Invisible Anapoles" (ANASTASIA), funded by Compagnia di San Paolo in the framework of Joint Projects for the Internationalization of Research.

#### REFERENCES

- [1] A. Petosa, *Dielectric Resonator Antenna Handbook*. Norwood, MA, USA: Artech House, 2007.
- [2] A. Petosa and A. Ittipiboon, "Dielectric resonator antennas: A historical review and the current state of the art," *IEEE Antennas Propag. Mag.*, vol. 52, no. 5, pp. 91–116, Oct. 2010.
- [3] R. K. Mongia and P. Bhartia, "Dielectric resonator antennas—A review and general design relations for resonant frequency and bandwidth," *Int. J. Microw. Millim.-Wave Comput.-Aided Eng.*, vol. 4, no. 3, pp. 230–247, 1994.
- [4] K. W. Leung, E. H. Lim, and X. S. Fang, "Dielectric resonator antennas: From the basic to the aesthetic," *Proc. IEEE*, vol. 100, no. 7, pp. 2181–2193, Jul. 2012.
- [5] H. Y. Lo, K. W. Leung, K. M. Luk, and E. K. N. Yung, "Low profile equilateral-triangular dielectric resonator antenna of very high permittivity," *Electron. Lett.*, vol. 35, no. 25, pp. 2164–2166, Dec. 1999.
- [6] A. Ittipiboon, R. K. Mongia, Y. M. M. Antar, P. Bhartia, and M. Cuhaci, "Aperture fed rectangular and triangular dielectric resonators for use as magnetic dipole antennas," *Electron. Lett.*, vol. 29, no. 23, pp. 2001–2002, Nov. 1993.
- [7] S. Maity and B. Gupta, "Approximate theoretical investigations on isosceles triangular dielectric resonator antennas and experimental validation," *IEEE Trans. Antennas Propag.*, vol. 66, no. 5, pp. 2640–2643, May 2018.
- [8] S. Maity and B. Gupta, "Theoretical investigations on equilateral triangular dielectric resonator antenna," *IET Microw., Antennas Propag.*, vol. 11, no. 2, pp. 184–192, 2017.
- [9] S. Maity and B. Gupta, "Experimental investigations on wideband triangular dielectric resonator antenna," *IEEE Trans. Antennas Propag.*, vol. 64, no. 12, pp. 5483–5486, Dec. 2016.
- [10] H. Y. Lo and K. W. Leung, "Excitation of low-profile equilateral-triangular dielectric resonator antenna using a conducting conformal strip," *Microw. Opt. Technol. Lett.*, vol. 29, no. 5, pp. 317–319, 2001.
- [11] R. Kumari, K. Parmar, and S. K. Behera, "A dual band triangular shaped DRA array for WLAN/WiMAX applications," in *Proc. Annu. IEEE India Conf.*, Hyderabad, India, Dec. 2011, pp. 1–4.
- [12] S. Fakhte and H. Oraizi, "Compact uniaxial anisotropic dielectric resonator antenna operating at higher order radiating mode," *Electron. Lett.*, vol. 52, no. 19, pp. 1579–1580, Aug. 2016.
- [13] S. Fakhte, H. Oraizi, and L. Matekovits, "High gain rectangular dielectric resonator antenna using uniaxial material at fundamental mode," *IEEE Trans. Antennas Propag.*, vol. 65, no. 1, pp. 342–347, Jan. 2017.
- [14] S. Fakhte and H. Oraizi, "Analysis and design of rectangular uniaxial and biaxial anisotropic dielectric resonator antennas," *Prog. Electromagn. Res. C*, vol. 62, pp. 43–50, 2016.
- [15] S. Fakhte, H. Oraizi, L. Matekovits, and G. Dassano, "Cylindrical anisotropic dielectric resonator antenna with improved gain," *IEEE Trans. Antennas Propag.*, vol. 65, no. 3, pp. 1404–1409, Mar. 2017.
- [16] R. E. Collin, "A simple artificial anisotropic dielectric medium," *IRE Trans. Microw. Theory Techn.*, vol. 6, no. 2, pp. 206–209, Apr. 1958.
- [17] H. S. Kirschbaum and S. Chen, "A method of producing broad-band circular polarization employing an anisotropic dielectric," *IRE Trans. Microw. Theory Techn.*, vol. 5, no. 3, pp. 199–203, Jul. 1957.
- [18] C. A. Balanis, *Advanced Engineering Electromagnetics*. New York, NY, USA: Wiley, 1989.
- [19] G. P. Junker, A. A. Kishk, A. W. Glisson, and D. Kajfez, "Effect of air gap on cylindrical dielectric resonator antenna operating in  $TM_{01}$  mode," *Electron. Lett.*, vol. 30, no. 2, pp. 97–98, Jan. 1994.
- [20] G. P. Junker, A. A. Kishk, A. W. Glisson, and D. Kajfez, "Effect of fabrication imperfections for ground-plane-backed dielectric-resonator antennas," *IEEE Antennas Propag. Mag.*, vol. 37, no. 1, pp. 40–47, Feb. 1995.
- [21] G. Drossos, Z. Wu, and L. E. Davis, "Aperture-coupled cylindrical dielectric resonator antenna," *Microw. Opt. Technol. Lett.*, vol. 20, no. 6, pp. 407–414, 1999.



**SAEED FAKHTE** was born in Amlash, Iran, in 1987. He received the B.Sc. degree from the Sharif University of Technology, Tehran, Iran, in 2009, and the M.Sc. and Ph.D. degrees in electrical engineering from the Iran University of Science and Technology, Tehran, Iran, in 2012 and 2017, respectively. From January 2016 to July 2016, he was a Visiting Ph.D. Student at the Politecnico di Torino, Torino, Italy. His research interests are in various areas of microwave and antenna engineering, such as dielectric resonator antennas, microstrip antennas, and microwave components. He has authored and co-authored over 10 papers in Peer-reviewed journals. He is currently a Researcher with the Politecnico di Torino, where he is involved in the area of the antenna development for RF applications. He has served as a Reviewer for the IEEE Transactions on Antennas and Propagation, the IEEE Antennas and Wireless Propagation Letters, the *IET Microwaves, Antennas and Propagation*, the *IET Electronic Letters*, the *International Journal of RF and Microwave Computer-Aided Engineering*, and other journals on antennas and electromagnetics.



ing, electromagnetic theory, and computational electromagnetics.

**IMAN ARYANIAN** was born in Iran in 1986. He received the B.Sc. degree in electrical engineering, and the M.Sc. and Ph.D. degrees in electrical communication engineering in 2008, 2010, and 2016, respectively, from the Amirkabir University of Technology, Tehran, Iran. He is currently an Assistant Professor with the Iran Telecommunication Research Center, Tehran. His research interests are in the areas of the reflectarray antenna, computational electromagnetic, semiconductor RF model-



**LADISLAU MATEKOVITS** (M'94–SM'11) received the degree in electronic engineering from the Institutul Politehnic din București, Romania, and the Ph.D. degree in electronic engineering from the Politecnico di Torino, Italy, in 1992 and 1995, respectively. Since 1995, he has continuously been with the Electronics Department, Politecnico di Torino, where he has been appointed as an Assistant Professor and also an Associate Professor in 2002 and 2014, respectively. In 2009, he has been a Marie Curie Fellow at Macquarie University, Sydney, NSW, Australia, for two years, where he is currently an Honorary Fellow. He authored over 300 publications in journals, conferences, workshops, and book chapters. His main research activities concern computational electromagnetics, optimization techniques, and active and passive metamaterials. He has delivered seminars on these topics all around the world, including Europe, USA, Australia, China, and Russia. He is a member of the Organizing Committee of the International Conference on Electromagnetics in Advanced Applications and the technical program committees of several conferences. He is a recipient of various awards, including the 1998 URSI Young Scientist Award and the Best AP2000 Oral Paper on Antennas at the ESA-EUREL Millennium Conference on Antennas & Propagation. He has been the Assistant Chairman and the Publication Chairman of the European Microwave Week 2002, Milan, Italy, and the General Chair of BodyNets 2016, Torino, Italy. He serves as an Associate Editor for the IEEE Antennas and Wireless Propagation Letters, the IEEE Access, *IET Microwaves, Antennas and Propagations*, and a reviewer for different journals.

...